JACS
JOURNAL OF THE AMERICAN CHEMICAL SOCIETY
Article
pubs.acs.org/JACS

Binary and Ternary Superlattices Self-Assembled from Colloidal Nanodisks and Nanorods

Taejong Paik,[†] Benjamin T. Diroll,[†] Cherie R. Kagan,[†,‡,§] and Christopher B. Murray*[,†,‡]

[†]Department of Chemistry, University of Pennsylvania, Philadelphia, Pennsylvania 19104, United States
[‡]Department of Materials Science and Engineering, University of Pennsylvania, Philadelphia, Pennsylvania 19104, United States
[§]Department of Electrical and Systems Engineering, University of Pennsylvania, Philadelphia, Pennsylvania 19104, United States

Supporting Information

ABSTRACT: Self-assembly of multicomponent anisotropic nanocrystals with controlled orientation and spatial distribution allows the design of novel metamaterials with unique shape- and orientation-dependent collective properties. Although many phases of binary structures are theoretically proposed, the examples of multicomponent assemblies, which are experimentally realized with colloidal anisotropic nanocrystals, are still limited. In this report, we demonstrate the formation of binary and ternary superlattices from colloidal two-dimensional LaF_3 nanodisks and one-dimensional CdSe/CdS nanorods via liquid interfacial assembly. The colloidal nanodisks and nanorods are coassembled into AB-, AB_2-, and AB_6-type binary arrays determined by their relative size ratio and concentration to maximize their packing density. The position and orientation of anisotropic nanocrystal building blocks are tightly controlled in the self-assembled binary and ternary lattices. The macroscopic orientation of the superlattices is further tuned by changing the liquid subphase used for self-assembly, resulting in the formation of lamellar-type binary liquid crystalline superlattices. In addition, we demonstrate a novel ternary superlattice self-assembled from two different sizes of nanodisks and a nanorod, which offers the unique opportunity to design multifunctional metamaterials.

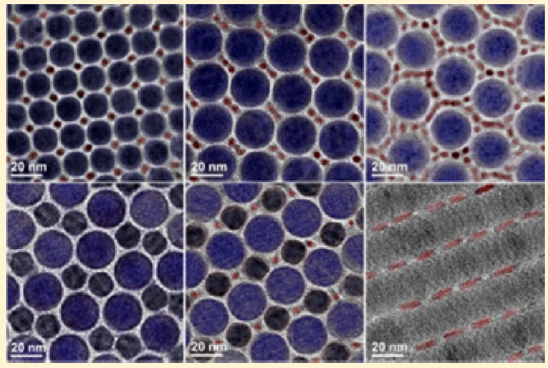

INTRODUCTION

Colloidal self-assembly of nanocrystals has tremendous potential to fabricate complex functional metamaterials structured at the nanoscale through a bottom-up approach.[1−4] When nanocrystals of various size, shape, and composition are self-assembled into ordered arrays, novel collective properties arise from the controlled coupling between the nanocrystals in the superlattices, which are governed by symmetry, coordination, interparticle spacing, order, and macroscopic orientation of the self-assembled structures.[5−7] Among various types of nanocrystal building blocks, anisotropic nanocrystals are particularly interesting due to their shape- and orientation-dependent properties.[8,9] For example, semiconducting CdSe nanorods[10] and nanoplatelets[11] exhibit shape-dependent polarized luminescence properties. In addition, Au nanorods[12] and $Cu_{2-x}S$ nanodisks[13] show orientation-dependent transverse and longitudinal plasmonic responses. For the design of optical and electrical devices, assembling anisotropic building blocks with controlled orientation, symmetry, periodicity, and valency is crucial to exploit their unique shape-dependent properties in devices.[14−18]

Many colloidal assembly approaches are employed to control the position and orientation of anisotropic nanocrystals, for example, templated assembly,[19−22] self-assembly in block copolymers,[23−25] Langmuir−Blodgett assembly,[26] electric-field assisted assembly,[27,28] and drying-mediated self-assembly.[29,30] Self-assembly of anisotropic colloidal nanocrystals into liquid crystalline structures is a promising route to control the spatial configuration as well as the orientation of nanocrystal building blocks over large areas.[31−33] Colloidal anisotropic nanocrystals, such as nanodisks and nanorods, are easily aligned to form self-assembled liquid crystalline superlattices with controllable orientation.[34−37] Liquid crystalline superlattices can also be assembled from different types of nanocrystal building blocks to form multicomponent systems, in which the position of one component can be directed by the anisotropic liquid crystalline superstructure.[2,38−43] The position and orientation of multicomponent anisotropic nanocrystals can be further tailored by designing different types of binary phases possessing unique symmetry, stoichiometry, and spatial coordination of the components in ordered arrays. Rich phase diagrams are theoretically proposed and understood by hard particle models,[44,45] or by the combination of particle−particle interactions driven by electrostatic force,[46,47] magnetic interaction,[48,49] and dipole−dipole or van der Waals interaction between particles or ligands on the particle surface.[50−53] In addition, the introduction of multiple anisotropic building blocks greatly expands the possible phase diagrams accessible for assembled structures.[54−57] Therefore, complex new

Received: March 28, 2015
Published: April 30, 2015

DOI: 10.1021/jacs.5b03234
J. Am. Chem. Soc. 2015, 137, 6662−6669

materials with emergent or collective properties and tailored superlattice structures can be designed de novo by the selection of appropriate building blocks.

Here, we report novel binary and ternary superlattices self-assembled from two colloidal anisotropic nanocrystals: two-dimensional nanodisks and one-dimensional nanorods. The nanorods and nanodisks are deposited to form superlattice thin films on glycol-type polar subphases via the liquid interfacial assembly technique.[6] We employ lanthanum trifluoride (LaF_3) nanodisks and CdSe/CdS nanorods as building blocks. By changing the relative size ratio and concentration of the nanodisks and nanorods and the subphases upon which the nanocrystals self-assemble, AB-, AB_2-, and AB_6-type columnar binary lattices and lamellar-type liquid crystalline superlattices are fabricated. Structural analysis shows these systems to be very densely packed. We speculate that the self-assembled structures maximize the packing density of the building blocks, hence increasing the free-volume entropy and minimizing the Helmholtz free energy. The position and orientation of colloidal nanodisks and nanorods are precisely controlled in the binary lattices preserving long-range orientational and positional order. In addition, we observe a novel ABC-type ternary superlattice self-assembled from two nanodisks and one nanorod, which is to our knowledge the first example of an ordered assembly formed from three anisotropic nanocrystals.

RESULTS AND DISCUSSION

Colloidal LaF_3 nanodisks are used as transparent dielectric nanocrystal building blocks for self-assembly. LaF_3 nanodisks are synthesized by a method previously reported in the literature with slight modification.[39] Transmission electron microscopy (TEM) (Figure 1a) shows nearly monodisperse LaF_3 nanodisks lying parallel to the substrate surface self-assemble into columnar hexagonal arrays. Wide-angle X-ray diffractions (XRD) of these nanodisks show sharp (100) and (300) diffraction peaks with trigonal crystal structures (JCPDS No. 32−0483), indicating that the nanodisks are truncated by the (001) plane and grow preferentially along the LaF_3 (100)-plane (Figure S1a,b, Supporting Information). Wide-angle selected-area electron diffraction (SAED) of self-assembled nanodisks shows relatively intense hexagonal electron diffraction spots representing the slight hexagonal faceting of the nanodisks (Figure S2).

The size, shape, and size distribution of nanodisks are confirmed by wide-angle and small-angle X-ray measurement and simulation. Experimentally measured X-ray diffraction patterns match simulation results for LaF_3 nanodisks that are 13.2 nm in diameter and 1.6 nm in thickness (Figure S1a). The size of nanodisks is further tunable by the controlled overcoating of additional layers on the core nanodisks by a seeded-growth reaction. After the overcoating, the size increases to about 22.3 nm in diameter with no noticeable change in thickness (Figure 1a, S1b), as corroborated by SAXS patterns and simulations.

Colloidal CdSe/CdS nanorods are used as a model one-dimensional building block because of their unique optical properties and shape uniformity. CdSe/CdS dot-in-rods are synthesized by a seeded growth method reported previously.[58] Figure 1b shows a representative TEM image of the synthesized CdSe/CdS nanorods used in this study. The length and diameter of the nanorods, which are characterized by X-ray measurement and simulation, are 15.1 and 3.8 nm, respectively (Figure S1c). Highly uniform nanorods self-assemble into

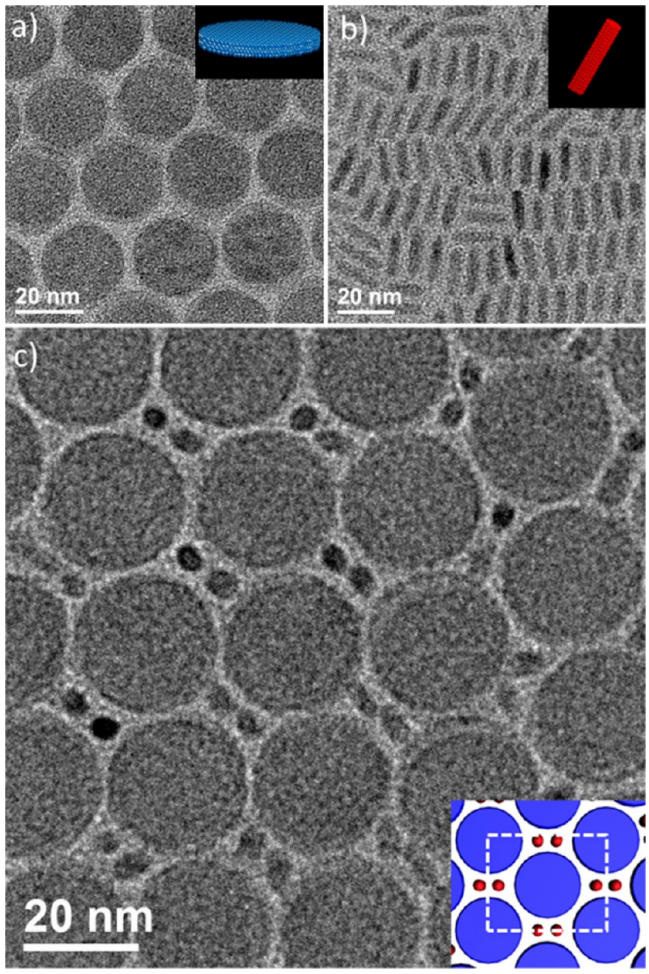

Figure 1. TEM images of anisotropic nanocrystal building blocks. (a) LaF_3 nanodisks (22.3 nm diameter with 1.6 nm thickness), (b) CdSe/CdS dot-in-rods (15.1 nm in length and 3.8 nm in diameter). (c) AB_2-type binary self-assembly of LaF_3 nanodisks and CdSe/CdS nanorods. Inset represents the schematic model of AB_2-type superlattice and unit cell.

smectic B liquid crystalline structures using the liquid interfacial assembly method on a diethylene glycol subphase. In some regions, the nanorods are vertically aligned in close-packed hexagonal arrays (homeotropic alignment, Figure S3a) and in other regions, the nanorods are horizontally aligned with respect to the substrate forming smectic liquid crystalline structures (heterogeneous alignment, Figure S3b,c).

To assemble binary superlattices from these shape-engineered building blocks, the mixed solution of LaF_3 nanodisks and CdSe/CdS dot-in-rods are similarly self-assembled via the liquid interfacial assembly technique using diethylene glygol as a subphase. The coassembly of nanodisks and nanorods into the binary lattices are observed with a small fraction of the single component arrays of nanodisks or nanorods. Figure 1c displays a TEM image of AB_2-type binary superlattices of large LaF_3 nanodisks (22.3 nm diameter × 1.6 nm thickness) and CdSe/CdS nanorods (15.1 nm length × 3.8 nm diameter). In the binary superlattices, nanodisks form columnar liquid crystalline structures by stacking out of the plane and two vertically aligned nanorods fill each interstitial site between the stacked columns of nanodisks. Four sets of two vertically aligned nanorods (dimers) are included in binary lattices with 4-fold symmetric positions around the columns.

DOI: 10.1021/jacs.5b03234
J. Am. Chem. Soc. 2015, 137, 6662−6669

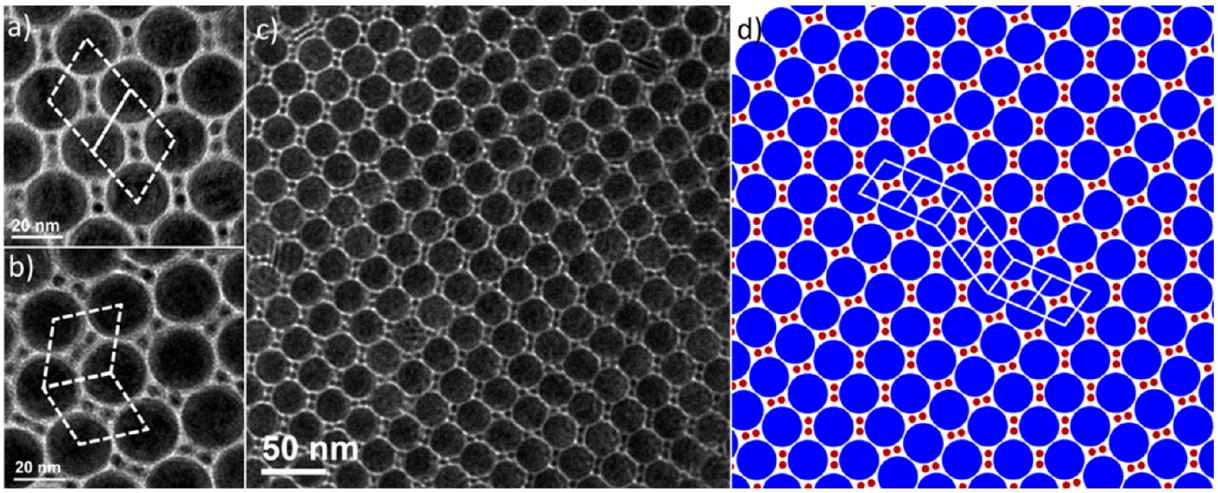

Figure 2. TEM images of AB_2-type binary superlattices. Colloidal LaF_3 nanodisks and CdSe/CdS nanorods are self-assembled with (a) D_{2h} point group symmetry and (b) C_{2v} point group symmetry. (c) Low magnification TEM image and (d) the structural model visualizing the twin boundary in the self-assembled AB_2-type superlattices.

To accommodate the inclusion of the nanorods in the interstitial sites of the 2-dimensional triangular Bravais lattice of the columns (Figure S2), the symmetry of self-assembled LaF_3 nanodisks is deformed to a centered rectangular lattice (Figure 1c, S4). Although the lattice structures formed by the binary mixture of nanodisks and nanorods are analyzed as two-dimensional lattice structures, the actual structures exhibit three-dimensional features with a stacking of nanodisks in each column. We observed that the number of nanodisks in the columns can be varied, as seen by the difference in contrast between the columns in TEM images (Figure S4a,b and c,d) The height of the columns can match the length of the vertically aligned nanorods (Figure S5b), consistent with as many as approximately 5 to 6 disks stacked in each single column in the binary assemblies.

Two possible configurations of the nanorod inclusion are observed in binary superlattices. One variant is that four sets of vertically aligned nanorod dimers around the columns are oriented into the same direction with D_{2h} point group symmetry, as depicted in Figure 2a. The second variant occurs when two sets of nanorod dimers are aligned at a 90° angle in the interstitial sites of nanodisk arrays with C_{2v} point group symmetry, as shown in Figure 2b, which has a mirror plane that intersects the center of the nanodisks. The simultaneous occurrence of both configurations during the self-assembly induces twin boundaries in the superlattice structures, as described in Figure 2c and 2d. This suggests that the energy barriers to formation for D_{2h} and C_{2v} symmetry arrays are comparable or within kT such that thermal fluctuations provide enough energy to produce both configurations.[59]

To understand the phase behavior of our binary superlattices, coassembly of nanorods with different sizes of LaF_3 nanodisks is performed. When the diameter of nanodisks used for self-assembly is decreased from 22.3 to 13.2 nm without changing the size of the nanorods, AB-type binary superlattices with *P4mm* symmetry[60] are observed predominantly where the nanorods are vertically aligned and doped into the interstices of LaF_3 nanodisk arrays, by deforming the triangular lattices into square lattices (Figure 3a–c). For nanodisks with the larger 22.3 nm diameter, as described previously, AB_2-type binary superlattices with C2mm symmetry[60] are predominantly formed where the two vertically aligned nanorods are placed at the interstices of the centered rectangular lattices (Figure 3d–f). By increasing the concentration of nanorods and using the same 22.3 nm diameter nanodisks and the nanorods, AB_6-type binary lattices with *P6mm* symmetry is observed, where the stacked nanodisks are assembled into hexagonal lattices while the vertically aligned nanorods are dodecagonally arrayed along the edge of nanodisk columns, as displayed in Figure 3g–i. The grain sizes of these AB_6-type binary structures extend over larger than 10 μm^2, as displayed in Figure 4, while maintaining their long-range orientational and positional orders.

The phase diagram of binary mixtures of hard disks has been investigated theoretically,[50,61,62] motivated by Fejes Tóth[63] and Liko et al.[64] The binary structures are expected from a theoretical model of space-filling, in which the two disk components are self-assembled into the two-dimensional binary lattices that maximize the packing density of the system. In our binary superlattices, all nanodisks and nanorods are aligned in the same crystallographic direction. Therefore, a top-view of AB-, AB_2-, and AB_6-type superlattices represents the binary disk arrays by treating the vertically aligned nanorods as second disks with small diameter. This provides guidance to explain the phase behaviors of our binary nanodisk-nanorod systems. Indeed, the experimental results represent the theoretical models where the two components are self-assembled into binary lattices maximizing space filling efficiency. AB-type binary arrangement is predicted to be stable in the range of $0.155 < \rho < 0.414$, where $\rho = r_{small}/r_{large}$, to maximize the packing density.[64] The diameter of small nanodisks and nanorods used for AB-type assembly, which are calculated by X-ray measurement and simulation, are 13.2 and 3.8 nm, respectively. Since our colloidal nanocrystals are coated with the long alkyl chain ligands, the effective size can be estimated by adding the thickness of the soft ligand shell, which is measured as the center-to-center distance of nanocrystals in the hexagonally ordered, single-component monolayer. The relative size ratio calculated by the effective sizes of nanocrystal building blocks is about 0.40, which falls into the range where AB-type structures with square lattices are favorably formed to maximize their space filling efficiency. Increasing size of the nanodisks to 22.3 nm, results in a relative size ratio of about 0.25, which is in the range where AB_2-type binary disk mixtures are expected to

DOI: 10.1021/jacs.5b03234
J. Am. Chem. Soc. 2015, 137, 6662–6669

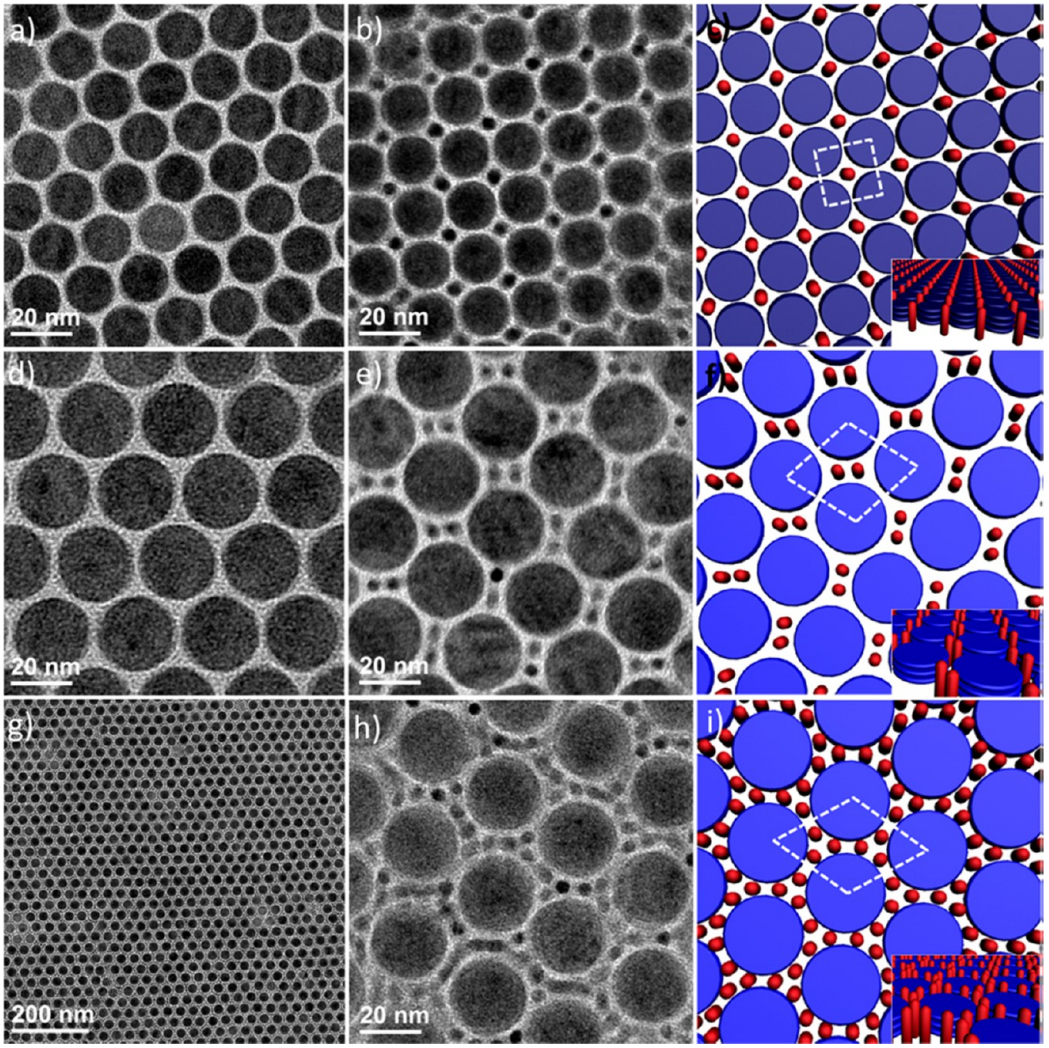

Figure 3. Self-assembled superlattices of nanodisks and nanorods depending on the relative size ratio and concentrations. TEM images of (a) a single component superlattice self-assembled from 13.2 nm LaF_3 nanodisks and (b) AB-type binary superlattice self-assembled from 13.2 nm LaF_3 nanodisks and CdSe/CdS nanorods and (c) the structural model of AB-type binary superlattice. (d) Single component superlattice self-assembled from 22.3 nm LaF_3 nanodisks and (e) AB_2-type superlattice self-assembled from 22.3 nm LaF_3 nanodisks and CdSe/CdS nanorods and (f) the structural model of AB_2-type binary superlattice. (g) Low magnification and (h) high magnification TEM images and (i) the structural model of AB_6-type superlattices self-assembled from 22.3 nm LaF_3 nanodisks and CdSe/CdS nanorods.

be stable and form centered rectangular lattices ($0.155 < \rho < 0.281$, Table 1).[64] This is confirmed by experimental observations showing predominant AB_2-type binary superlattices (Figure 3d–f). Increasing the concentration of nanorods but maintaining the relative size ratio results in the formation of AB_6-type binary superlattices to accommodate the building blocks and maximize the packing density, which is predicted be stable in the range of $0.101 < \rho < 0.349$.[64] Table 1 summarizes the ranges of stability for different binary lattices. Although space-filling models of binary disk arrays can explain the observed binary superlattices, the formation of these structures may involve contributions from many additional interactions such as free volume entropy and the enthalpic interactions including dipole–dipole,[65] van der Waals,[66] an interaction between the ligands on the surfaces,[52] and depletion attraction interactions.[67] The understanding of these interactions may enable a variety of novel binary structures with different types of anisotropic nanocrystals to be precisely designed.

The ternary nanocrystal superlattices formed from three spherical nanocrystals have been observed by Vanmaekelbergh et al.[68] and Murray et al.;[69] however, the example of the ternary superlattices composed of three different colloidal nanocrystals is still rare and from anistropic building blocks is unprecedented. Here, we obtained new ternary superlattices by coassembly of three different anisotropic nanocrystal building blocks, small and large LaF_3 nanodisks, and CdSe/CdS nanorods. To investigate the self-assembly behavior of three components, nanocrystal solutions used for AB-type superlattice (small nanodisks and nanorods) and AB_2-type superlattice (large nanodisks and nanorods) are mixed together in a 1:1 volume ratio and dropped onto the surface of diethylene glycol. Locally, phase segregation to AB-type and AB_2-type binary superlattices is observed as displayed in Figure 5a, which reflects the energetic preference of both binary lattices over single component arrays. In addition to the AB- and AB_2-type superlattices described above, we observed the binary assembly of two different nanodisks, in which nanodisks of each diameter are stacked to form columns and self-

DOI: 10.1021/jacs.5b03234
J. Am. Chem. Soc. 2015, 137, 6662–6669

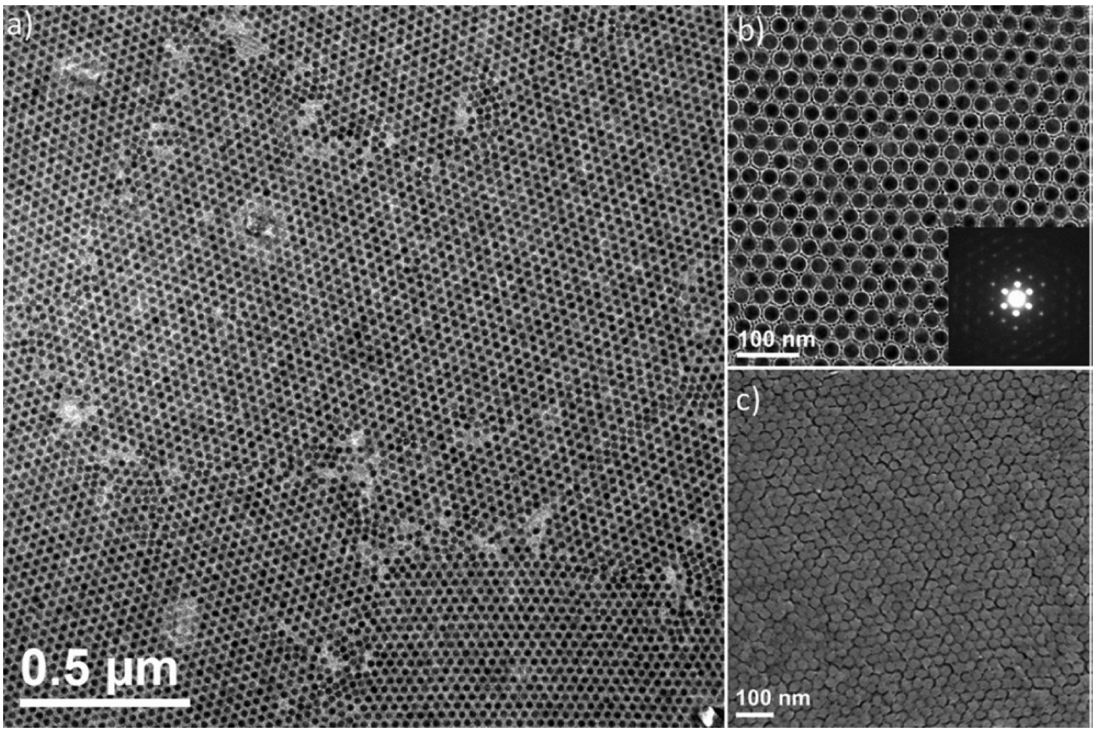

Figure 4. (a) Low- (b) high-magnification TEM images and (c) SEM image of AB_6-type binary superlattices self-assembled from large LaF_3 nanodisks and CdSe/CdS nanorods. Inset in (b) represents the small-angle SAED pattern of AB_6-type binary superlattice.

Table 1. Range of Stability Calculated As the Two-Dimensional Binary Lattices of Hard Disks[a]

stoichiometry	range of stability	experimental size ratio (ρ)	magic size ratio
AB	$0.155 < \rho < 0.414$	0.397	0.414
AB_2	$0.155 < \rho < 0.281$	0.251	0.281
AB_6	$0.101 < \rho < 0.349$	0.251	0.349

[a]Adapted from references 51, 61, 62, 64.

assembled into an AB-type binary superlattice having an oblique 2-D Bravis lattice (Figure 5b,c). We also observe ABC-type ternary superlattices with a centered rectangular lattice (Figure 5d–f), in which stacked columns of small and large nanodisks are self-assembled into centered rectangular lattices and vertically aligned CdSe nanorods are located in the interstices between stacked nanodisk columns of small LaF_3 nanodisks, as displayed in Figure 5d–f.

The orientation of binary liquid crystalline structures is further tuned by changing the subphase upon self-assembly. When ethylene glycol is used as a subphase for self-assembly instead of a diethylene glycol subphase, lamellar-type liquid crystalline structures are predominantly formed with a small area of AB_2-type binary lattice formation (Figure 6, S5, S6). In the lamellar-type superlattices, nanodisks stand edge-on on the substrates and stack to form one-dimensional strings by face-to-face interactions. These strings are simultaneously self-assembled into extended smectic liquid crystalline arrays. In the presence of colloidal nanorods, building blocks are coassembled into liquid crystalline binary lattices where nanorods lie parallel to the substrates and are placed between two strings of LaF_3 nanodisk arrays. The tip-to-tip distances between the nanorods is close to the length of the interdigitated ligands bound on the surface. The nanorods are close-packed into one-dimensional arrays leaving a minimal space except for the surface ligands. The trench formed between the arrays of nanodisk strings provides free space to incorporate the nanorod building blocks, similar to the examples of nanoplate/nanosphere[39] and nanorod/nanosphere[41] binary systems. This trench allows for the alignment of nanorods along the orientation of lamellar liquid crystalline structures. At the edge of superlattice, it is observed that the nanorods nearby a nanodisk arrays are already aligned without the presence of the neighboring columns (Figure S6d) indicating that the presence of the nanodisk assemblies induces preferential alignment of the nanorods along the direction of the nanodisk lamellar. Since dielectric LaF_3 nanodisks are used as building blocks, liquid crystalline binary structures may be utilized as a template directing one-dimensional building blocks into long-range ordered, close-packed periodic arrays.

■ CONCLUSION

We demonstrate that mixtures of two and three different anistropically shaped colloidal nanocrystals coassembly into binary and ternary superlattices respectively with long-range orientational and positional order. By changing the relative size and concentration of LaF_3 nanodisks and CdSe/CdS nanorods, we synthesized AB_2-type, AB_6-type, and two AB-type binary superlattices as well as an ABC-type ternary superlattice, which are driven to maximize the packing density. The orientation of superlattice structures is tunable by changing the subphases upon which self-assembly occurs resulting in the formation of lamellar-type binary liquid crystalline superlattices. In this structure, the pitch size of one-dimensionally aligned nanorods would be further tuned in the binary lattices by changing the diameter of synthesized nanodisks. The demonstration of binary and ternary superlattices constructed from anisotropic building blocks shows shape-engineering of nanocrystals can be used to access new phases/structures, which allows for the

DOI: 10.1021/jacs.5b03234
J. Am. Chem. Soc. 2015, 137, 6662–6669

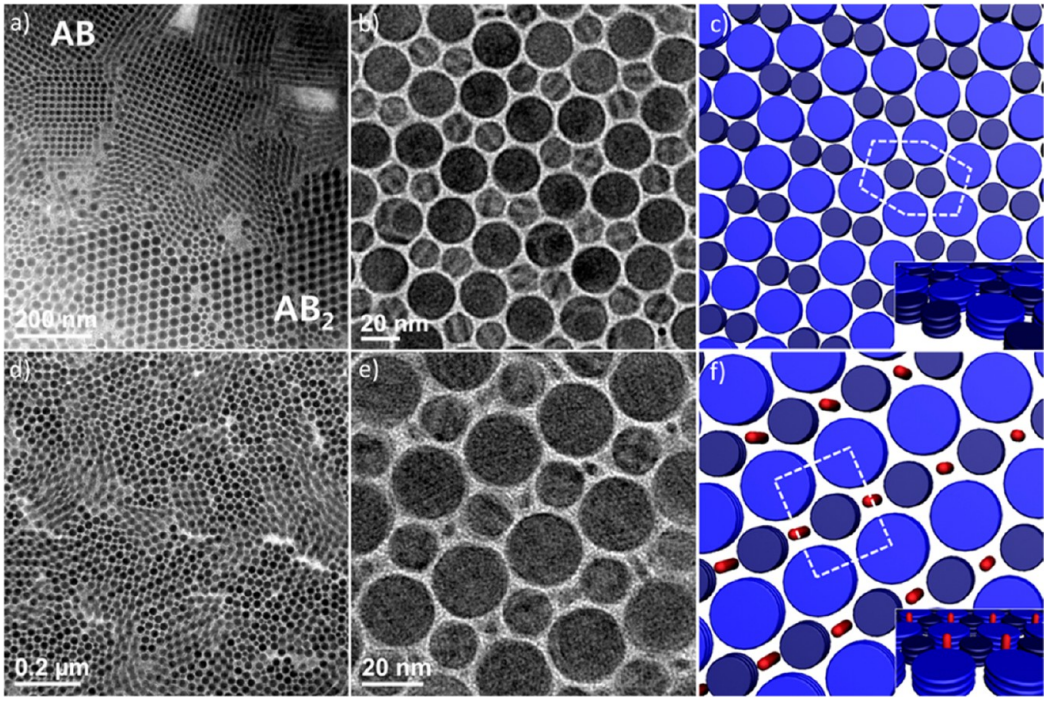

Figure 5. (a) TEM images of self-assembled structures from small and large LaF_3 nanodisks, and CdSe/CdS nanorods. Phase-segregation to AB-type and AB_2-type superlattices is observed. (b) TEM image and (c) the structural model of an AB-type superlattice self-assembled from small LaF_3 and large LaF_3 nanodisks. (d) Low magnification, (e) high magnification TEM images and (f) the structural model of ABC-type superlattices self-assembled from small and large LaF_3 nanodisks and CdSe/CdS nanorods.

design of novel functional metamaterials by tailoring superlattice structures.

EXPERIMENTAL SECTION

Materials. All chemicals are used as purchased without any further purification. Lanthanum(III) oxide (99.9%), lithium fluoride (99.99%), cadmium oxide (99.99%), oleic acid (technical grade, 90%), and 1-octadecene (technical grade, 90%) are all purchased from Sigma-Aldrich. Diethylene glycol and ethylene glycol are purchased from Fisher scientific. Trifluoroacetic acid (99.5+%) is purchased from Alfa Aesa. Lanthanum trifluoroacetate ($LaTFA_3$) precursors are synthesized by refluxing 10 g of lanthanum oxide in 100 mL of trifluoroacetic acid and water mixture (50/50 vol %).

Synthesis of LaF_3 Nanodisks. Colloidal LaF_3 nanodisks are synthesized according to the procedure previously reported with slight modification.[39] Briefly, LiF (6 mmol) and $LaTFA_3$ (2 mmol) are added oleic acid and 1-octadecene mixture (50/50 vol %) in a 125 mL three-neck flask. The reaction mixture is degassed at 125 °C for 2 h and then the solution is heated to 290 °C under N_2 environment at a rate of 15 °C/min and maintained at this temperature for 4 h. Next, the reaction solution is purified by precipitating nanocrystals in excess ethanol and centrifugation at 4000 rpm for 2 min. Purification process is conducted 2 times. After purification, hexane is added into the precipitates to dissolve nanocrystals. Residual lithium fluoride, which is not dissolved in nonpolar solvents, is simply removed by centrifugation at 3000 rpm for 2 min.

Seed-Growth Overcoating of LaF_3 Nanodisks. Mixture of nanocrystal solution, 3 mmol of LiF, and 1 mmol of $LaTFA_3$ are added into a 125 mL three-neck flask filled with oleic acid and 1-octadecene mixture (50/50 vol %) and degassed at 125 °C for 2 h. and then the reaction mixture is heated to 280 °C at a rate of 15 °C/min under N_2 environment and maintained at this temperature for 2 h. The purification is conducted with the same method described earlier.

Synthesis of CdSe/CdS Dot-in-Rods. Synthesis of CdSe/CdS dot-in-rod samples followed literature procedures.[23,54]

Binary Assembly of LaF_3 Nanodisks and CdSe/CdS Nanorods. The liquid interfacial assembly is performed by following the procedure reported in literature.[6] Briefly, a Teflon well is filled with diethylene glycol or ethylene glycol subphases. And then, 30 μL of the nanocrystal mixtures in hexane is dropped onto the surface of subphases in the Teflon well and slowly dried by covering a glass slide on the interface. Once nanocrystal solution on the interface is fully dried to form the membrane, resulting films are transferred to carbon-coated TEM grids for microscopic analysis. The TEM grids are further dried in the vacuum chamber to remove residual subphases. Concentration of nanocrystals used for self-assemblies is (1.6 mg + 8 mg)/mL of hexane (small LaF_3 and CdSe/CdS nanorods) for AB-type superlattices, (1.1 mg + 8 mg)/mL of hexane (large LaF_3 and CdSe/CdS nanorods) for AB_2-type superlattices, (1.1 mg + 16 mg)/mL (large LaF_3 and CdSe/CdS nanorods) for AB_6-type superlattices, and (1.6 mg + 1.1 mg + 8 mg)/mL (small LaF_3, large LaF_3, and CdSe/CdS nanorods) for ABC-type superlattices.

Characterization. TEM images and electron diffraction patterns are collected using a JEM-2100 microscope equipped operating at 200 kV. Scanning electron microscopy (SEM) images are collected on a JEOL 7500F HRSEM. Powder X-ray diffraction measurements are conducted using a Rigaku Smartlab high-resolution diffractometer equipped with a 2.2 kW sealed tube generator. X-ray diffraction patterns are collected using concentrated nanocrystal solutions filled in a glass capillary enabling the diffraction patterns to be measured for randomly oriented nanodisks. Small-angle X-ray scattering measurement are performed at the Multi-Angle X-ray Scattering Facility at the University of Pennsylvania. The size and shape information are extracted from X-ray simulation of wide-angle X-ray diffraction patterns and small-angle X-ray scattering (SAXS) results.[39,70] The atomic coordinates and shape information on the nanodisks, which are constructed from the monoclinic LaF_3 unit cell (JCPDS no. 32−0483) and the statistical size analysis from TEM images, are entered into the Debye formula to generate the simulated X-ray patterns.

DOI: 10.1021/jacs.5b03234
J. Am. Chem. Soc. 2015, 137, 6662−6669

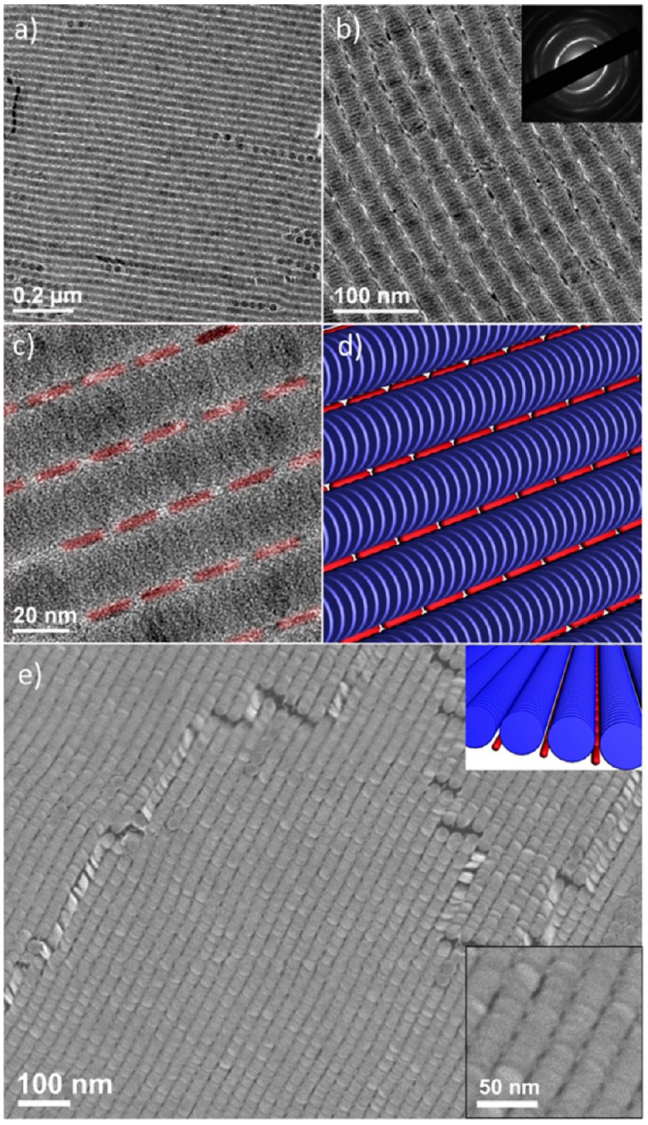

Figure 6. (a–c) TEM images and (d) the structural model of lamellar-type binary superlattices self-assembled from large LaF_3 and CdSe/CdS nanorods. Inset in (b) is the wide-angle selected area electron diffraction pattern The red colors in (c) mark the position of the CdSe/CdS nanorods. (e) SEM image of lamellar-type binary superlattices. Inset is high-magnification SEM image and the structural model.

■ ASSOCIATED CONTENT

Supporting Information

SAXS and WAXS patterns, additional TEM and SEM images. The Supporting Information is available free of charge on the ACS Publications website at DOI: 10.1021/jacs.5b03234.

■ AUTHOR INFORMATION

Corresponding Author

*cbmurray@sas.upenn.edu

Notes

The authors declare no competing financial interest.

■ ACKNOWLEDGMENTS

We thank Dr. Paul Heiney for an analytical support on small-angle X-ray scattering measurements. We thank the Office of Naval Research Multidisciplinary University Research Initiative Award No. ONR-N00014-10-1-0942 for primary support for the synthesis of LaF_3 nanodisks, performing the self-assembly studies, and the microscopic analysis. Synthesis of CdSe/CdS dot-in-rods, small- and wide-angle X-ray characterizations, and X-ray simulation were supported by the U.S. Department of Energy Office of Basic Energy Sciences, Division of Materials Science and Engineering under Award No. DE-SC0002158. C.R.K. is thankful for the support of the Stephen J. Angello Professorship. C.B.M. is grateful for the support of the Richard Perry University Professorship.

■ REFERENCES

(1) Murray, C. B.; Kagan, C. R.; Bawendi, M. G. *Annu. Rev. Mater. Sci.* **2000**, *30*, 545–610.
(2) Shevchenko, E. V.; Talapin, D. V.; Kotov, N. A.; O'Brien, S.; Murray, C. B. *Nature* **2005**, *439*, 55–59.
(3) Grzelczak, M.; Vermant, J.; Furst, E. M.; Liz-Marzán, L. M. *ACS Nano* **2010**, *4*, 3591–3605.
(4) Macfarlane, R. J.; Lee, B.; Jones, M. R.; Harris, N.; Schatz, G. C.; Mirkin, C. A. *Science* **2011**, *334*, 204–208.
(5) Urban, J. J.; Talapin, D. V.; Shevchenko, E. V.; Kagan, C. R.; Murray, C. B. *Nat. Mater.* **2007**, *6*, 115–121.
(6) Dong, A.; Chen, J.; Vora, P. M.; Kikkawa, J. M.; Murray, C. B. *Nature* **2010**, *466*, 474–477.
(7) Ye, X.; Chen, J.; Diroll, B. T.; Murray, C. B. *Nano Lett.* **2013**, *13*, 1291–1297.
(8) Kan, S.; Mokari, T.; Rothenberg, E.; Banin, U. *Nat. Mater.* **2003**, *2*, 155–158.
(9) Jones, M. R.; Macfarlane, R. J.; Prigodich, A. E.; Patel, P. C.; Mirkin, C. A. *J. Am. Chem. Soc.* **2011**, *133*, 18865–18869.
(10) Hu, J.; Li, L.-s.; Yang, W.; Manna, L.; Wang, L.-w.; Alivisatos, A. P. *Science* **2001**, *292*, 2060–2063.
(11) Cassette, E.; Mahler, B.; Guigner, J.-M.; Patriarche, G.; Dubertret, B.; Pons, T. *ACS Nano* **2012**, *6*, 6741–6750.
(12) Jana, N. R.; Gearheart, L.; Murphy, C. J. *J. Phys. Chem. B* **2001**, *105*, 4065–4067.
(13) Hsu, S.-W.; On, K.; Tao, A. R. *J. Am. Chem. Soc.* **2011**, *133*, 19072–19075.
(14) Rizzo, A.; Nobile, C.; Mazzeo, M.; Giorgi, M. D.; Fiore, A.; Carbone, L.; Cingolani, R.; Manna, L.; Gigli, G. *ACS Nano* **2009**, *3*, 1506–1512.
(15) Rivest, J. B.; Swisher, S. L.; Fong, L.-K.; Zheng, H.; Alivisatos, A. P. *ACS Nano* **2011**, *5*, 3811–3816.
(16) Alvarez-Puebla, R. A.; Agarwal, A.; Manna, P.; Khanal, B. P.; Aldeanueva-Potel, P.; Carbó-Argibay, E.; Pazos-Pérez, N.; Vigderman, L.; Zubarev, E. R.; Kotov, N. A.; Liz-Marzán, L. M. *Proc. Natl. Acad. Sci. U. S. A.* **2011**, *108*, 8157–8161.
(17) Jones, M. R.; Macfarlane, R. J.; Lee, B.; Zhang, J.; Young, K. L.; Senesi, A. J.; Mirkin, C. A. *Nat. Mater.* **2010**, *9*, 913–917.
(18) Walker, D.; Browne, K. P.; Kowalczyk, B.; Grzybowski, B. A. *Angew. Chem., Int. Ed.* **2010**, *49*, 6760–6763.
(19) Yin, Y.; Lu, Y.; Gates, B.; Xia, Y. *J. Am. Chem. Soc.* **2001**, *123*, 8718–8729.
(20) Xia, Y.; Yin, Y.; Lu, Y.; McLellan, J. *Adv. Funct. Mater.* **2003**, *13*, 907–918.
(21) Rupich, S. M.; Castro, F. C.; Irvine, W. T. M.; Talapin, D. V. *Nat. Commun.* **2013**, *5*, 5045.
(22) Greybush, N. J.; Saboktakin, M.; Ye, X.; Giovampaola, C. D.; Oh, S. J.; Berry, N. E.; Engheta, N.; Murray, C. B.; Kagan, C. R. *ACS Nano* **2014**, *8*, 9482–9491.
(23) Thorkelsson, K.; Mastroianni, A. J.; Ercius, P.; Xu, T. *Nano Lett.* **2012**, *12*, 498–504.
(24) Zhang, Q.; Gupta, S.; Emrick, T.; Russell, T. P. *J. Am. Chem. Soc.* **2006**, *128*, 3898–3899.
(25) Deshmukh, R. D.; Liu, Y.; Composto, R. J. *Nano Lett.* **2007**, *7*, 3662–3668.
(26) Kim, F.; Kwan, S.; Akana, J.; Yang, P. *J. Am. Chem. Soc.* **2001**, *123*, 4360–4361.

DOI: 10.1021/jacs.5b03234
J. Am. Chem. Soc. 2015, 137, 6662–6669

(27) Ryan, K. M.; Mastroianni, A.; Stancil, K. A.; Liu, H.; Alivisatos, A. P. *Nano Lett.* **2006**, *6*, 1479−1482.
(28) Carbone, L.; Nobile, C.; Giorgi, M. D.; Sala, F. D.; Morello, G.; Pompa, P.; Hytch, M.; Snoeck, E.; Fiore, A.; Franchini, I. R.; Nadasan, M.; Silvestre, A. F.; Chiodo, L.; Kudera, S.; Cingolani, R.; Krahne, R.; Manna, L. *Nano Lett.* **2007**, *7*, 2942−2950.
(29) Talapin, D. V.; Shevchenko, E. V.; Murray, C. B.; Kornowski, A.; Förster, S.; Weller, H. *J. Am. Chem. Soc.* **2004**, *126*, 12984−12988.
(30) Baker, J. L.; Widmer-Cooper, A.; Toney, M. F.; Geissler, P. L.; Alivisatos, A. P. *Nano Lett.* **2010**, *10*, 195−201.
(31) Gabriel, J.-C. P.; Davidson, P. *Top. Curr. Chem.* **2003**, *226*, 119−172.
(32) Wu, K.-J.; Chu, K.-C.; Chao, C.-Y.; Chen, Y.-F.; Lai, C.-W.; Kang, C.-C.; Chen, C.-Y.; Chou, P.-T. *Nano Lett.* **2007**, *7*, 1908−1913.
(33) Lynch, M. D.; Patrick, D. L. *Nano Lett.* **2002**, *2*, 1197−1201.
(34) Saunders, A. E.; Ghezelbash, A.; Smilgies, D.-M.; Sigman, M. B.; Korgel, B. A. *Nano Lett.* **2006**, *6*, 2959−2963.
(35) Cao, Y. C. *J. Am. Chem. Soc.* **2004**, *126*, 7456−7457.
(36) Zhang, Y.-W.; Sun, X.; Si, R.; You, L.-P.; Yan, C.-H. *J. Am. Chem. Soc.* **2005**, *127*, 3260−3261.
(37) Ye, X.; Collins, J. E.; Kang, Y.; Chen, J.; Chen, D. T. N.; Yodh, A. G.; Murray, C. B. *Proc. Natl. Acad. Sci. U. S. A.* **2010**, *107*, 22430−22435.
(38) Sánchez-Iglesias, A.; Grzelczak, M.; Pérez-Juste, J.; Liz-Marzán, L. M. *Angew. Chem., Int. Ed.* **2010**, *49*, 9985−9989.
(39) Paik, T.; Ko, D.-K.; Gordon, T. R.; Doan-Nguyen, V.; Murray, C. B. *ACS Nano* **2011**, *5*, 8322−8330.
(40) Ming, T.; Kou, X.; Chen, H.; Wang, T.; Tam, H.-L.; Cheah, K.-W.; Chen, J.-Y.; Wang, J. *Angew. Chem., Int. Ed.* **2008**, *47*, 9685−9690.
(41) Ye, X.; Millan, J. A.; Engel, M.; Chen, J.; Diroll, B. T.; Glotzer, S. C.; Murray, C. B. *Nano Lett.* **2013**, *13*, 4980−4988.
(42) Paik, T.; Murray, C. B. *Nano Lett.* **2013**, *13*, 2952−2956.
(43) Nagaoka, Y.; Wang, T.; Lynch, J.; LaMontagne, D.; Cao, Y. C. *Small* **2012**, *8*, 843−846.
(44) Murray, M. J.; Sanders, J. V. *Philos. Mag. A* **1980**, *42*, 721−740.
(45) Filion, L.; Dijkstra, M. *Phys. Rev. E: Stat., Nonlinear, Soft Matter Phys.* **2009**, *79*, 046714.
(46) Kalsin, A. M.; Fialkowski, M.; Paszewski, M.; Smoukov, S. K.; Bishop, K. J. M.; Grzybowski, B. A. *Science* **2006**, *312*, 420−424.
(47) Bartlett, P.; Campbell, A. I. *Phys. Rev. Lett.* **2005**, *95*, 128302.
(48) Singh, G.; Chan, H.; Baskin, A.; Gelman, E.; Repnin, N.; Král, P.; Klajn, R. *Science* **2014**, *345*, 1149−1153.
(49) Ahniyaz, A.; Sakamoto, Y.; Bergström, L. *Proc. Natl. Acad. Sci. U. S. A.* **2007**, *104*, 17570−17545.
(50) Law, A. D.; Buzza, D. M. A.; Horozov, T. S. *Phys. Rev. Lett.* **2011**, *106*, 128302.
(51) Fornleitner, J.; Verso, F. L.; Kahl, G.; Likos, C. N. *Langmuir* **2009**, *25*, 7836−7846.
(52) Ye, X.; Chen, J.; Engel, M.; Millan, J. A.; Li, W.; Qi, L.; Xing, G.; Collins, J. E.; Kagan, C. R.; Li, J.; Glotzer, S. C.; Murray, C. B. *Nat. Chem.* **2013**, *5*, 446−473.
(53) Leunissen, M. E.; Christova, C. G.; Hynninen, A.-P.; Royall, P.; Campbell, A. I.; Imhof, A.; Dijkstra, M.; Roij, R. v.; Blaaderen, A. v. *Nature* **2005**, *437*, 235−240.
(54) Millan, J. A.; Ortiz, D.; Anders, G. v.; Glotzer, S. C. *ACS Nano* **2014**, *8*, 2918−2928.
(55) Glotzer, S. C.; Solomon, M. J. *Nat. Mater.* **2007**, *6*, 557−562.
(56) Damasceno, P. F.; Engel, M.; Glotzer, S. C. *Science* **2012**, *337*, 453−457.
(57) Sacanna, S.; Pine, D. J. *Curr. Opin. Colloid Interface Sci.* **2011**, *16*, 96−105.
(58) Miszta, K.; Graaf, J. d.; Bertoni, G.; Dorfs, D.; Brescia, R.; Marras, S.; Ceseracciu, L.; Cingolani, R.; Roij, R. v.; Dijkstra, M.; Manna, L. *Nat. Mater.* **2011**, *10*, 872−876.
(59) Elechiguerra, J. L.; Reyes-Gasga, J.; Yacaman, M. J. *J. Mater. Chem.* **2006**, *16*, 3906−3919.
(60) Tschierske, C. *Chem. Soc. Rev.* **2007**, *26*, 1930−1970.
(61) Assoud, L.; Messina, R.; Löwen, H. *Europhys. Lett.* **2007**, *80*, 48001.
(62) Uche, O. U.; Stillinger, F. H.; Torquato, S. *Physica A* **2004**, *342*, 428−446.
(63) Tóth, L. F. *Regular Figures*; Macmillan: New York, 1964.
(64) Likos, C. N.; Henley, C. L. *Philos. Mag. B* **1993**, *68*, 85−113.
(65) Li, L.-S.; Alivisatos, A. P. *Adv. Mater.* **2003**, *15*, 408−411.
(66) Titov, A. V.; Kral, P. *Nano Lett.* **2008**, *8*, 3605−3612.
(67) Baranov, D.; Fiore, A.; Huis, M. v.; Giannini, C.; Falqui, A.; Lafont, U.; Zandbergen, H.; Zanella, M.; Cingolani, R.; Manna, L. *Nano Lett.* **2010**, *10*, 743−749.
(68) Evers, W. H.; Friedrich, H.; Filion, L.; Dijkstra, M.; Vanmaekelbergh, D. *Angew. Chem., Int. Ed.* **2009**, *48*, 9655−9657.
(69) Dong, A.; Ye, X.; Chen, J.; Murray, C. B. *Nano Lett.* **2011**, *11*, 1804−1809.
(70) Murray, C. B.; Norris, D. J.; Bawendi, M. G. *J. Am. Chem. Soc.* **1993**, *115*, 8706−8715.

DOI: 10.1021/jacs.5b03234
J. Am. Chem. Soc. 2015, 137, 6662−6669